VĚDECKÉ SPISY VYSOKÉHO UČENÍ TECHNICKÉHO V BRNĚ

Edice PhD Thesis, sv. 739

ISSN 1213-4198

Ing. Anna Sterkhova

Modelling of Pulse Propagation in Nonlinear Photonic Structures

VYSOKÉ UČENÍ TECHNICKÉ V BRNĚ
FAKULTA STROJNÍHO INŽENÝRSTVÍ
ÚSTAV FYZIKÁLNÍHO INŽENÝRSTVÍ

Ing. Anna Sterkhova

MODELLING OF PULSE PROPAGATION IN NONLINEAR PHOTONIC STRUCTURES

MODELOVÁNÍ ŠÍŘENÍ PULZNÍHO ZÁŘENÍ
V NELINEÁRNÍCH FOTONICKÝCH STRUKTURÁCH

Zkrácená verze Ph.D. Thesis

Obor:	Fyzikální a materiálové inženýrství
Školitel:	prof. RNDr. Jiří Petráček, Dr.
Oponenti:	Mgr. Ota Samek, Dr.
	doc. Ing. Ivan Richter, Dr.
Datum obhajoby:	4. dubna 2014

Keywords:
optical waveguides, numerical modelling, integrated optics, ring resonators, coupled resonant structures, coupled mode theory, nonlinear optics, Kerr nonlinearity, bistability, self-pulsing, chaos.

Klíčová slova:
optické vlnovody, numerické modelování, integrovaná optika, prstencové rezonátory, vázané rezonanční struktury, teorie vázáných modů, nelineární optika, kerrovska nelinearita, bistabilita, samopulzace, chaos.

The full version of the Ph.D. thesis is available in the Institute of Physical Engineering of Faculty of Mechanical Engineering, Brno University of Technology.

ISBN 978-80-214-4944-2
ISSN 1213-4198

Contents

1 Introduction **5**
1.1 Motivation 5
1.2 Objectives and scope of the thesis 5

2 Coupled-equation (CE) technique **6**
2.1 Derivation of coupled mode equations 6
2.2 Formulation 8
2.3 Stability analysis 10
2.4 Accuracy analysis 12
2.5 Numerical examples 13

3 Discrete-equation (DE) technique **16**
3.1 Formulation for waveguide 17
3.2 Formulation for ADF/APF structure 17
3.3 Non-instantaneous response of the system 20
3.4 Numerical examples 20

4 Conclusions **24**

References **26**

1 Introduction

Modern technology tends to minimization. However, globalization demands every-day growing data exchange. That is why, the most of changes are in the communication sphere, where the demands of faster data transfer, better signal quality and more effective data storage are very high. Recently there was a substantial increase in number of investigations and studies of the optical devices as effective communication technology of the future and in some cases of our present.

The speed of signal processing is crucial for present amount of data exchange. On our days electrical based signal processing is used. The speed of the latter can be significantly increased with the all-optical device. That means a device, in which the signal is processed with light only. Light waves, however, can interact with each other only with the presence of nonlinearity. That is why nonlinear photonic devices are under the intensive study. The ultimate aim is to use the devices as optical switches, amplifiers, logical gates, optical memory, *etc.*

1.1 Motivation

The most promising structures which can be used as a reliable configuration in the telecommunication and signal processing applications are structures, based on resonant cavities. These devices usually consist of one or several cavities which are coupled to bus waveguide. In the thesis, the focus will be made on the structures with cavities formed by a looped waveguides - microring (or ring) resonators. The resulting structures are referred as coupled ring resonators (CRRs).

To understand and describe the principles of light propagation in optical devices the Maxwell's equations (or a wave equation) are a common starting point for analytical investigations. Furthermore, considering the all-optical devices, it is necessary to take into account nonlinear optical phenomena. In this regime, however, it is very difficult to find rigorous solutions of the aforesaid equations analytically. To simulate and optimize the processes occurring in the CRRs the powerful numerical techniques are needed. There are a number of numerical methods, which are based on physical intuition of the processes taking place in the optical devices. The most commonly used rigorous numerical simulation technique is a finite difference time-domain technique (FD-TD). However this method, being rigorous, is rather involved and demand large computer resources. The alternative to FD-TD are various approximate methods, based on an appropriate physical models. If the Kerr-nonlinear structures are under consideration, the simulation can be based on a coupled equation method or a transfer matrix method. This approach allows to develop simple approximative methods, which will combine advantages of mentioned simulation techniques but will not be so time-consuming as, for example, FD-TD method.

1.2 Objectives and scope of the thesis

This work is focused on the development and implementation of novel and effective methods for simulation of pulse propagation in nonlinear photonic structures, mainly in the CRR structures. The CRR with the Kerr nonlinearity is under investigation.

The first objective is to develop a suitable physical model based on the coupled mode theory that will describe propagation of optical pulses in Kerr-nonlinear waveguide structures.

The second objective is to investigate possible numerical schemes for solving of the resulting equations. The emphasis will be made on the stability and efficiency of the developed schemes.

Then the method should be extended to the simulation of resonant structures based on CRRs.

The third objective is application of the developed method to the study of nonlinear properties of the CRR structures. The investigation will be focused on the dynamical behavior with the aim to study the generation of the optical pulses from the continuous input (self-pulsing regime).

The choice of investigated structures is explained by the various and interesting phenomena which occur in CRRs. These structures also allow easy modification of linear spectral characteristic, which have however significant impact on the nonlinear behavior of the structure. There are intense researches of CRRs nonlinear behavior, of new materials, which will allow more precise production, lower side-walls roughness and smaller cavity sizes [1]. All these factors indicate not only theoretical, but also practical interest to CRRs and their implementation. Especially, when the dynamics of the nonlinear propagation in the resonant structures is studied, the newly developed methods can be a promising counterpart to the existing numerical techniques. That is why we believe, that the developed simulation techniques will be useful in study of novel and interesting effects occurring in nonlinear photonic structures.

The scope of the thesis encompasses the derivation of two novel simulation methods and its application to the resonant structures based on the ring resonators. The derivation of the method starts with the pulse propagation in a single waveguide. Then the coupling between two waveguides, separated by a finite distance, in a linear case is considered. The model is then extended for nonlinear case. In a method these two types of equations (for a single waveguide and for waveguide coupler) are combined for simulation of pulse propagation in different types of CRR. The developed methods are applied to several different geometries of CRR and the results are compared with the results provided by currently used simulation techniques in order to check the new methods accuracy.

2 Coupled-equation (CE) technique

2.1 Derivation of coupled mode equations

Coupled mode theory is commonly used for theoretical description of waveguide couplers. In this section the derivation of coupled equations between the modes of two parallel waveguides in nonlinear case is presented.

Let us start from a single waveguide. The pulse propagation in such a waveguide can be described by equation, [2]:

$$\frac{\partial A}{\partial z} + \frac{1}{v_g}\frac{\partial A}{\partial t} + \frac{\alpha}{2}A = i\gamma|A|^2 A, \tag{2.1}$$

where v_g is the group velocity; γ is a nonlinear parameter. $A(z,t)$ is the slowly varying pulse envelope. The slowly varying envelope approximation (SVEA) $\frac{\partial^2 A}{\partial t^2} \to 0$ was used for the derivation of the Eq. (2.1).

When two single waveguides are separated by a finite distance, the physical overlap of the mode wave functions is present, the modes may be coupled [2], [3]. This effect found a number of useful applications in optical communications, such as power coupling and switching, [4], [5].

Let us consider two dielectric waveguides. The modes of each waveguide can be determined as

$$\tilde{\mathbf{E}}_a = \mathcal{E}_a(x,y)\exp(i\beta_a z) \tag{2.2}$$

$$\tilde{\mathbf{E}}_b = \mathcal{E}_b(x,y)\exp(i\beta_b z), \tag{2.3}$$

where $\mathcal{E}_m(x,y)$ is spatial electric mode distribution and β_m is mode-propagation constant of the m^{th} waveguide; $m = a, b$. With the presence of overlap the electric field of a general wave propagation in the coupled-waveguide structure is assumed as

$$\tilde{\mathbf{E}}(\mathbf{r},\omega) = [\tilde{A_a}(z,\omega)\mathcal{E}_a(x,y) + \tilde{A_b}(z,\omega)\mathcal{E}_b(x,y)]\exp(i\beta z), \tag{2.4}$$

where $\tilde{\mathbf{E}}(\mathbf{r},\omega)$, $\tilde{A_a}(z,\omega)$ and $\tilde{A_b}(z,\omega)$ are Fourier transform of the $\mathbf{E}(\mathbf{r},t)$, $A_a(z,t)$ and $A_b(z,t)$ with respect to time. $A_a(z,t)$ and $A_b(z,t)$ are pulse envelopes of waveguide a or b respectively. The individual modes of waveguides are strongly coupled with each other:

$$\frac{d\tilde{A_a}}{dz} = i\kappa_{ab}\tilde{A_b}\exp\left(i(\beta_a - \beta_b)z\right) + i\kappa_{aa}\tilde{A_a} \tag{2.5}$$

$$\frac{d\tilde{A_b}}{dz} = i\kappa_{ba}\tilde{A_a}\exp\left(-i(\beta_a - \beta_b)z\right) + i\kappa_{bb}\tilde{A_b} \tag{2.6}$$

where coupling coefficient κ is defined as:

$$\kappa_{ab} = \frac{\omega}{4}\varepsilon_0 \iint \varepsilon_a^* \cdot \Delta n_a^2(x,y)\varepsilon_b \mathrm{d}x\mathrm{d}y \tag{2.7}$$

$$\kappa_{aa} = \frac{\omega}{4}\varepsilon_0 \iint \varepsilon_a^* \cdot \Delta n_b^2(x,y)\varepsilon_a \mathrm{d}x\mathrm{d}y \tag{2.8}$$

$$a \neq b, \qquad a,b = 1,2$$

The spatial distribution of modes $\mathcal{E}_m(x,y)$ is obtained by solving the Helmholtz equation, [6]. It satisfies the following equation:

$$\frac{\partial^2 \mathcal{E}_m}{\partial x^2} + \frac{\partial^2 \mathcal{E}_m}{\partial y^2} + [n^2(x,y)k_0^2 - \beta_m^2]\mathcal{E}_m = 0, \tag{2.9}$$

where refractive index $n(x,y) = n_0$ elsewhere in the $(x-y)$ plane except the $m-th$ waveguide region, where it is larger by the constant amount. The solution of Eq. (2.9) can be found in [2].

Due to the overlap between two modes the mode amplitudes A_1 and A_2 while propagating along the corresponding waveguide vary with the distance z. To find their evolution with the distance z Eq. (2.4) is substituted into Helmholtz equation, multiplied the resulting equation by $\mathcal{E}_1^*$ or $\mathcal{E}_2^*$, use Eq. (2.9) and integrated over the entire $(x-y)$ plane. The resulting set of a frequency-domain coupled-mode equations can be converted to the time domain:

$$\frac{\partial A_1}{\partial z} + \frac{1}{v_g}\frac{\partial A_1}{\partial t} = i\kappa A_2 + i\gamma|A_1|^2 A_1, \tag{2.10}$$

$$\frac{\partial A_2}{\partial z} + \frac{1}{v_g}\frac{\partial A_2}{\partial t} = i\kappa A_1 + i\gamma|A_2|^2 A_2, \tag{2.11}$$

where the symmetrical waveguides were considered ($\kappa_{ab} = \kappa_{ba} \equiv \kappa$). For more detail see the full version of the thesis.

Let us consider the structure shown in the Fig. 1. It is single ring resonator coupled to the bus waveguide. Let $f(z,t)$ and $g(z,t)$ be correspondingly mode amplitudes in bus and ring waveguides propagating along the z axis. Let us focus on the coupling region of these waveguides. The

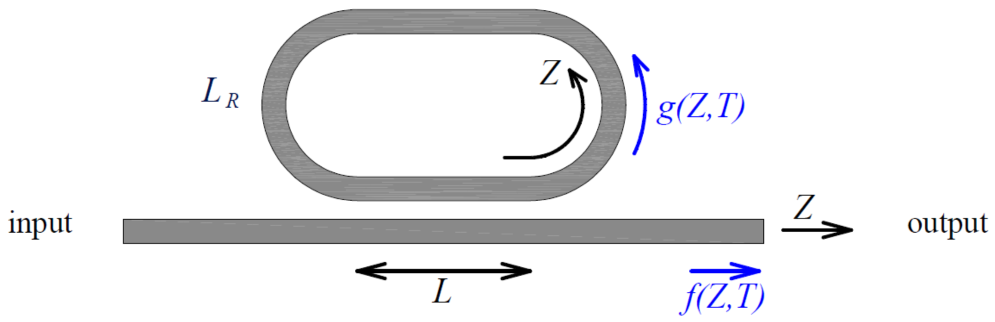

Figure 1: Schematic image of waveguide coupled to a ring

propagation of coupled modes is described by Eqs. (2.10) and (2.11). Let us now introduce new dimensionless time and spatial variables:

$$Z = zk_0, \qquad T = t\omega. \tag{2.12}$$

Hence, the Eqs. (2.10) and (2.11) are

$$\frac{\partial f}{\partial Z} + n_g \frac{\partial f}{\partial T} = i\kappa' g + in_2|f|^2 f \tag{2.13}$$
$$\frac{\partial g}{\partial Z} + n_g \frac{\partial g}{\partial T} = i\kappa' f + in_2|g|^2 g, \tag{2.14}$$

where κ' is the normalized coupling coefficient between waveguides, defined as $\kappa' = \kappa/k_0$ and $n_g = c/v_g$ is mode group index, n_2 is effective value of nonlinear Kerr index, defined as $n_2 = \gamma/k_0$.

In general, κ is the function of z. CE method enables the calculation of arbitrary dependence $\kappa(Z)$. We will assume the value of κ' inside of the coupling region to be constant.

2.2 Formulation

In the previous section the coupled equations (2.13) and (2.14) for a waveguide coupler were derived. In this section the formulation of CE method will be explained on the examples of a single waveguide and a waveguide coupler.

Waveguide

Partial differential equations (PDEs) can be solved numerically by different methods. Most important ones are finite element, spectral and variational methods [7]. The main problem of numerical methods, however, is the stability. That is why an up-wind method, schematically shown in Fig. 2 is the most suitable one for numerical simulation of PDEs which describe wave propagations, due to its stability, [7].

Let us consider a single lossless waveguide. Hence, the coupling coefficient $\kappa' = 0$ and the Eq. (2.13) becomes (compare with Eq. (2.1)):

$$\frac{\partial f}{\partial Z} + n_g \frac{\partial f}{\partial T} = in_2|f|^2 f. \tag{2.15}$$

where Z and T are defined in Eq. (2.12).

To solve numerically the Eq. (2.15) equally spaced points along both the T- and the Z-axes were chosen, Fig. 2:

$$\begin{aligned} Z_j &= Z_0 + j\Delta Z, \quad j = 0,1,\ldots,J, \\ T_n &= T_0 + n\Delta T, \quad n = 0,1,\ldots,N. \end{aligned}$$

The main difference of up-wind scheme from the other ones is in finding the adverted quantity of sought-for function in point j for positive velocity v only with the help of mesh point $j+1$. Hence, the function $f(Z,T)$ from Eq. (2.15) according to the up-wind scheme will be defined as:

$$n_g \frac{f_j^{n+1} - f_j^n}{\Delta T} = -\frac{f_j^n - f_{j-1}^n}{\Delta Z}. \tag{2.16}$$

Substituting $f(Z,T)$ into Eq. (2.15) we get:

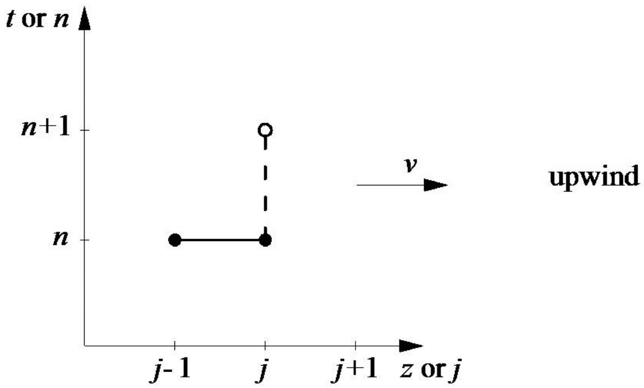

Figure 2: Up-wind scheme

$$n_g \frac{f_j^{n+1} - f_j^n}{\Delta T} + \frac{f_j^n - f_{j-1}^n}{\Delta Z} = i n_2 \left| \frac{f_j^n + f_{j-1}^n}{2} \right|^2 \left(\frac{f_j^n + f_{j-1}^n}{2} \right), \tag{2.17}$$

The choice of average value of the terms on the RHS of Eq. (2.17) is explained in Section 2.4. After simple algebra the previous equation becomes

$$f_j^{n+1} - f_j^n = -\alpha(f_j^n - f_{j-1}^n) + i\beta |f_j^n + f_{j-1}^n|^2 (f_j^n + f_{j-1}^n), \tag{2.18}$$

where

$$\alpha = \frac{\Delta T}{n_g \Delta Z}, \quad \beta = \frac{n_2 \Delta T}{8 n_g}. \tag{2.19}$$

Waveguide coupler

Let us now consider a waveguide coupler. We assume both waveguides to be single mode with the same mode effective index which is equal to the mode group index n_g. Let $f(Z,T)$ and $g(Z,T)$ represent the dimensionless mode field envelope in the waveguide 1 and 2 respectively. Equations (2.13) and (2.14) after using up-wind scheme are:

$$f_j^{n+1} - f_j^n = -\alpha(f_j^n - f_{j-1}^n) + i\gamma(g_j^n + g_{j-1}^n) + i\beta |f_j^n + f_{j-1}^n|^2 (f_j^n + f_{j-1}^n) \tag{2.20}$$

$$g_j^{n+1} - g_j^n = -\alpha(g_j^n - g_{j-1}^n) + i\gamma(f_j^n + f_{j-1}^n) + i\beta |g_j^n + g_{j-1}^n|^2 (g_j^n + g_{j-1}^n), \tag{2.21}$$

where $\gamma = \kappa \Delta T/(2n_g)$.

In order to solve the coupled system of Eqs. (2.13) and (2.14), it is necessary to know initial conditions. They, of course, are different for a various structure geometries.

2.3 Stability analysis

For methods using time domain for calculation of field evolution it is essential to determine stability condition, [8], [9], [10]. In those kind of methods wave propagation velocity in one-dimensional grid is determined with the help of distance ΔZ and time step ΔT. However, for time step ΔT there is a boundary, beyond which the numerical method is no longer stable.

It is well known that the up-wind differencing scheme for a single waveguide in linear case (in our case in Eqs. (2.20) and (2.21) $\gamma = 0$, $\beta = 0$) is numerically stable if the Courant condition is satisfied, [7]:

$$\frac{|v|\Delta t}{\Delta Z} \leq 1 \tag{2.22}$$

Let us now find stability condition for linear case of a waveguide coupler (in Eqs. (2.20) and (2.21) $\gamma \neq 0$, $\beta = 0$). For the studied case the von Neumann stability analysis was applied. The solution of coupled equations (2.20) and the (2.21) can be written in a vector form:

$$\begin{bmatrix} f_j^n \\ g_j^n \end{bmatrix} = \xi^n \exp(ikj\Delta Z) \begin{bmatrix} f^0 \\ g^0 \end{bmatrix}, \tag{2.23}$$

where f^0 and g^0 are assumed to be constant in space and time. Substituting Eq. (2.23) into Eq. (2.21) ($\beta = 0$) we will get the homogeneous vector equation

$$\begin{bmatrix} 1-\alpha(1-\exp(ik\Delta Z))-\xi & i\gamma(1+\exp(-ik\Delta Z)) \\ i\gamma(1+\exp(-ik\Delta Z)) & 1-\alpha(1-\exp(ik\Delta Z))-\xi \end{bmatrix} \cdot \begin{bmatrix} f^0 \\ g^0 \end{bmatrix} = \begin{bmatrix} 0 \\ 0 \end{bmatrix} \tag{2.24}$$

The solution can be found only if the determinant of the matrix, Eq. (2.24) equals to zero. This condition leads to the roots of the determinant

$$\xi = 1-\alpha(1-\exp(ik\Delta Z)) \pm i\gamma(1+\exp(-ik\Delta Z)) \tag{2.25}$$

From Eq. (2.23) it is evident that scheme will be stable if the condition $|\xi| \leq 1$ is satisfied for any k. Solving of the inequality leads to the stability condition for the linear case:

$$\gamma \leq \sqrt{\frac{1-\alpha}{2}}. \tag{2.26}$$

The graphical representation of the stability condition (2.26) can be seen in the Fig. 3.

To solve the remaining nonlinear case of the problem, the system of equations (2.20) and (2.21) was linearized. The principle of solving is analogous to the linear case and gives the additional stability criterion for the nonlinear case (the main stability condition is a Courant one, (2.22)):

$$\gamma + C \leq \sqrt{\frac{1-\alpha}{2}}, \quad \text{where} \quad C = \frac{n_2 \Delta T}{2n_g} I_{\max}. \tag{2.27}$$

$I_{\max}$ is maximum of values $|f_j^n|^2$ and $|g_j^n|^2$. The graph of the last expression is identical to the graph for the linear case (Fig. 3); on the vertical axis in nonlinear case will be $(\gamma + C)$.

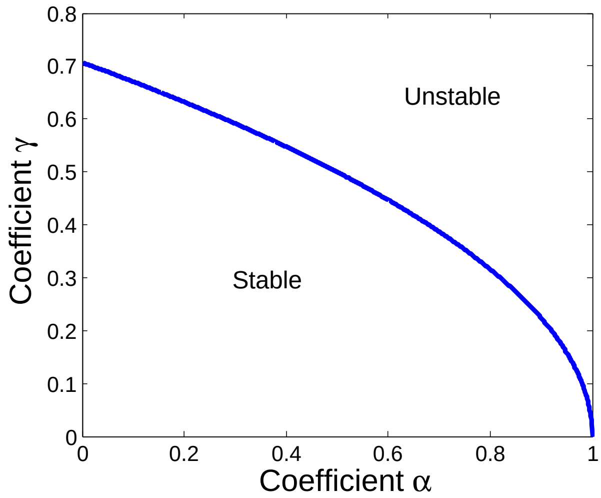

Figure 3: Graphical representation of stability condition (2.26) in linear case, [8]

The condition (2.27) can be rewritten into the following form:

$$\left[\frac{\arcsin(s)}{L} + n_2 I_{\max}\right] \Delta Z \leq \frac{\sqrt{2(1-\alpha)}}{\alpha}. \tag{2.28}$$

Note, that $n_2 I_{\max}$ is maximum of nonlinear change of effective index over the structure. In typical calculations $n_2 I_{\max} < 10^{-3}$; $\alpha = 0.9$ and $\Delta Z < 2\pi$. Thus, for small s and for long L inequality (2.28) is well satisfied. The opposite case (large s and short L) needs more attention; $n_2 I_{\max}$ can be negligible and the condition takes this form:

$$\frac{L}{\Delta Z} \geq \arcsin(s) \frac{\alpha}{\sqrt{2(1-\alpha)}}. \tag{2.29}$$

The criterion is illustrated in Fig. 4 for different values of the coefficient α.

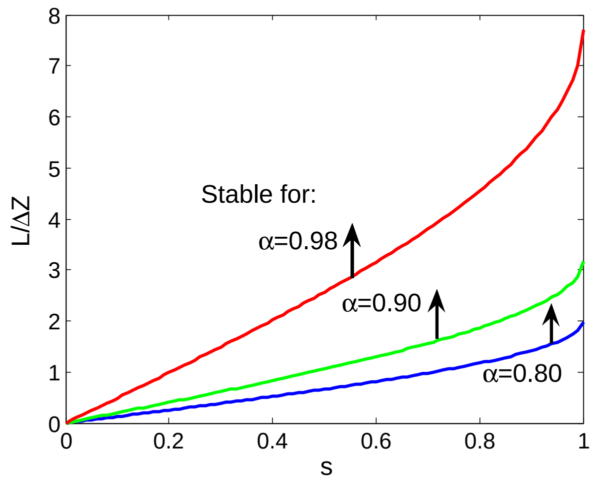

Figure 4: The graphical representation of the stability condition (2.29), [8]

2.4 Accuracy analysis

The form of the discrete representation of the RHS of Eqs. (2.13) or (2.14) follows from our numerical experiments. We have analyzed the linear problem (i. e. $\beta = 0$) and have chosen the presented formulation from the following alternatives of the second and third terms of RHS of Eqs. (2.20) or (2.21) correspondingly:

1. $(g_j^n + g_{j-1}^n)$, $(f_j^n + f_{j-1}^n)$,
2. $2g_j^n$, $2f_{j-1}^n$,
3. $2g_{j-1}^n$, $2f_j^n$,
4. $2g_j^n$, $2f_j^n$.

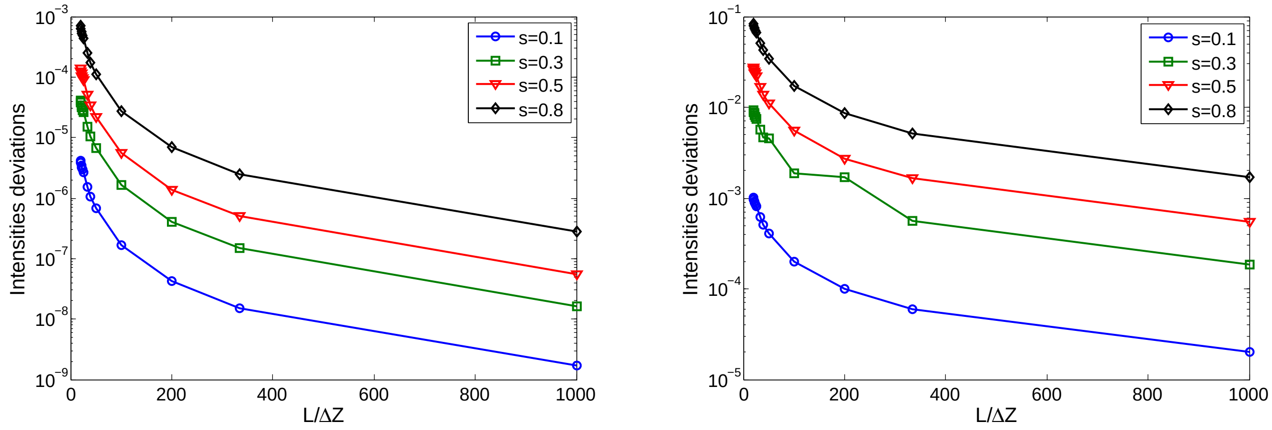

(a) Variant 1 (b) Variant 4

Figure 5: Relative intensity deviations for the alternative formulations of the second term on the RHS of Eqs. (2.20) and (2.21). The calculations were performed for various values of the coupling coefficient κ, wavelength $\lambda = 1.5\,\mu$m, and coupler length $10\,\mu$m, [11].

In order to choose the most suitable form, we considered the coupler configuration with an input as a monochromatic wave. In this case ($\beta = 0$, $(\partial/\partial T) = 0$, $\kappa = \text{const}$) we can compare the theoretical and numerical results and assess the accuracy of the CE technique. Let us calculate the output intensities in both waveguides analytically for the case $f(Z = 0, T) = f_0 = \text{const}$ and $g(Z = 0, T) = 0$:

$$|f(L,T)|^2 = |f_0|^2[1 - \sin^2(\kappa Z)] \tag{2.30}$$

$$|g(L,T)|^2 = |f_0|^2 \sin^2(\kappa Z). \tag{2.31}$$

We compared the deviations of the numerically calculated intensity and analytical results provided by Eqs. (2.30) and (2.31). Let us examine the first and the forth variant, Fig. 5. The relative errors of the forth variant are 100 times bigger than the ones of the first variant. The second and the third alternatives show results similar to the forth variant (they are not shown in the Fig. 5). By these calculations the most accurate scheme formulation was found (the variant 1). Hence, this scheme will be chosen for the CE method.

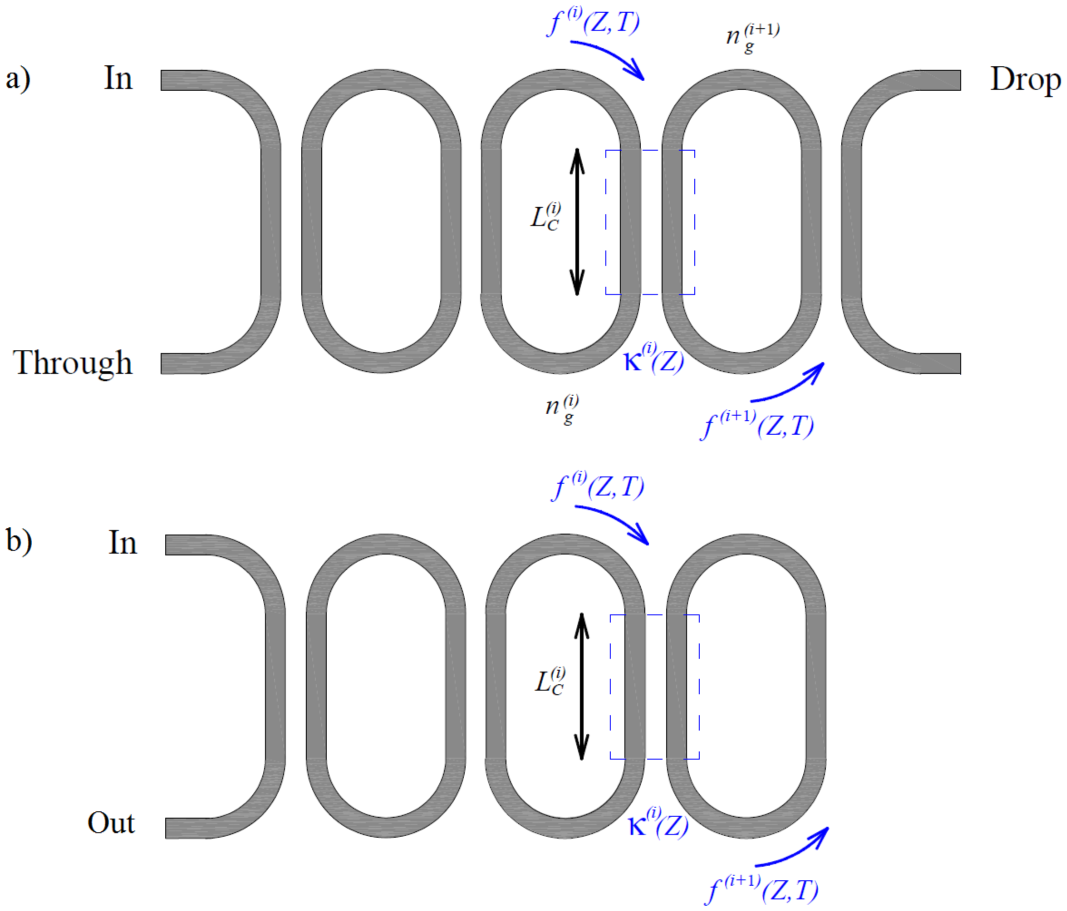

Figure 6: The ADF (a) and APF (b) configuration consisting of 3 coupled microrings

2.5 Numerical examples

ADF with several cavities

Let us consider the structure schematically shown in Fig. 6, (a). This add-drop filter (ADF) consists of 3 identical rings. ADF is the structure consisting of one or several ring resonators coupled to two waveguides. Generally, it is well-known, that structures with coupled cavities can be optimized for obtaining desired (e.g. flat-top) linear response; for structures with identical rings such optimization is done by suitable selection of coupling parameters $\kappa^{(i)}(Z)$, [12]. For the studied structure the parameters are: ring circumferences are $L = (7.0 + 13\pi)\,\mu$m. The optimized for flat response coupling coefficients $\kappa^{(0)}(Z) = \kappa^{(3)}(Z) = 0.4668$ and $\kappa^{(1)}(Z) = \kappa^{(2)}(Z) = 0.099$, are taken from [13]. All coupling lengths are $L_C^{(i)} = 3.5\,\mu$m. Mode effective indices, $n_g^{(i)} = 4.25$, and Kerr-indices are the same in all waveguides.

Figure 7 shows spectral dependencies of drop port transmission near resonance wavelength $\lambda \approx 1.5640\ \mu$m for various levels of nonlinearity. To obtain the Fig. 7 two method were used: Transfer matrix method (TMM) and CE. The principle of TMM is based on the knowing of the input field, then the output field can be calculated with the help of matrix operation.

As expected, nonlinearity shifts spectra towards longer wavelengths and group delay is increased near band edge for $\lambda > \lambda_r$. For a stable solutions both methods show the same results, shown by solid

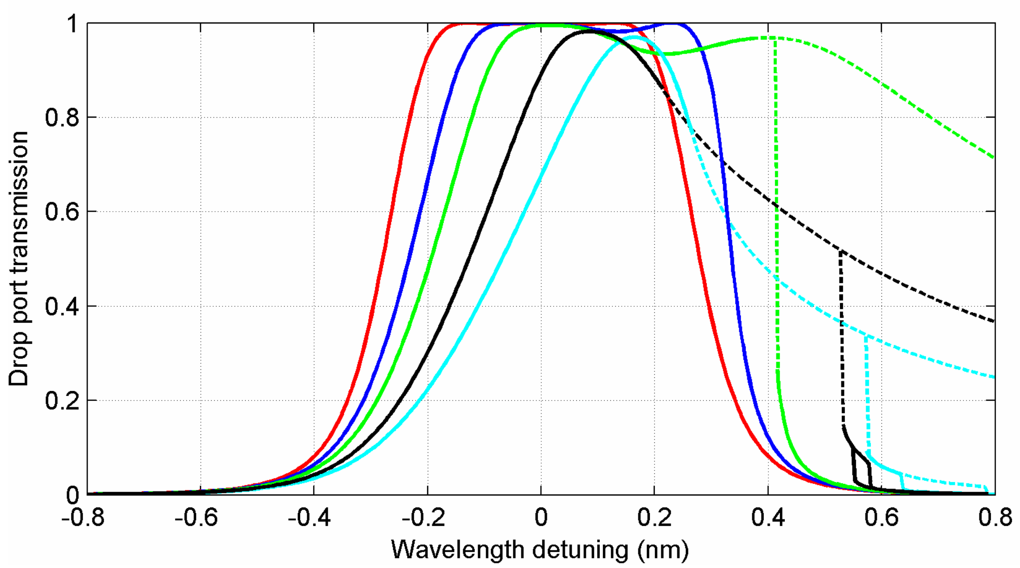

Figure 7: Drop port transmission vs. detuning from resonance wavelength for various values of normalized input intensity (curves have values of $n_2 I_{in} \times 10^5$ from left to right 0, 2, 4, 8 and 12). Solid lines represent stable solutions obtained by CE, dashed lines represent unstable solutions calculated by TMM, [15]

lines. Unstable solutions (shown by dashed lines) in Fig. 7 were obtained by TMM method. Despite these solutions fulfill stability condition $dI_{drop}/dI_{in} > 0$ and suggest that bistability may occur for $\lambda > \lambda_r$, they are not stable. This conclusion is confirmed by CE calculation, [14].

In this spectral regime CE method shows that solutions exhibit self-pulsing behavior, illustrated in Fig. 8. Self-pulsing is a regime, when the system responses with a train of pulses on a continuous input signal. Note that shape of the pulses at the through and drop ports, their amplitudes and periods depend on the normalized intensity in the steady state and detuning from resonance wavelength. For example, as illustrated in Fig. 8, period of the pulses decreases with increasing nonlinearity. More detailed discussion about self-pulsing behaviors of the ring resonators is presented in the Section 3.

APF with several cavities

For the next simulation the structure shown in Fig. 6, (b) is considered. The all pass filter (APF) structure has one or several coupled rings and only one bus waveguide, coupled to the side ring. For the numerical calculation all three microrings of APF are supposed to be identical with circumferences 50 μm. All coupling lengths are 5.0μm and the coupling coefficients are $\kappa^{(0)}(Z) = 0.5$ and $\kappa^{(1)}(Z) = \kappa^{(2)}(Z) = 0.1$. Mode effective indices, $n_g^{(i)} = 3.0$, and Kerr-indices are the same in all waveguides.

Figure 9 presents steady-state solutions obtained by the TMM and indicates regions in which the solutions are unstable. The unstable solutions were found with the help of technique, which is described in the Section 3.3. The nonlinear characteristic was calculated for wavelength $\lambda = 1.5005\,\mu m$ (above the resonance $\lambda_r = 1.5000\mu$m), $n_2 I_3$ is the normalized intensity in the ring. Unstable solutions are identified by linear stability analysis [14].

CE technique was used for obtaining the time-dependent solutions. Namely, we are interested in self-pulsing and chaotic solutions, which are obtained for constant input. (During the calculation, the input intensity is first gradually increased or decreased to the desired value and then kept constant).

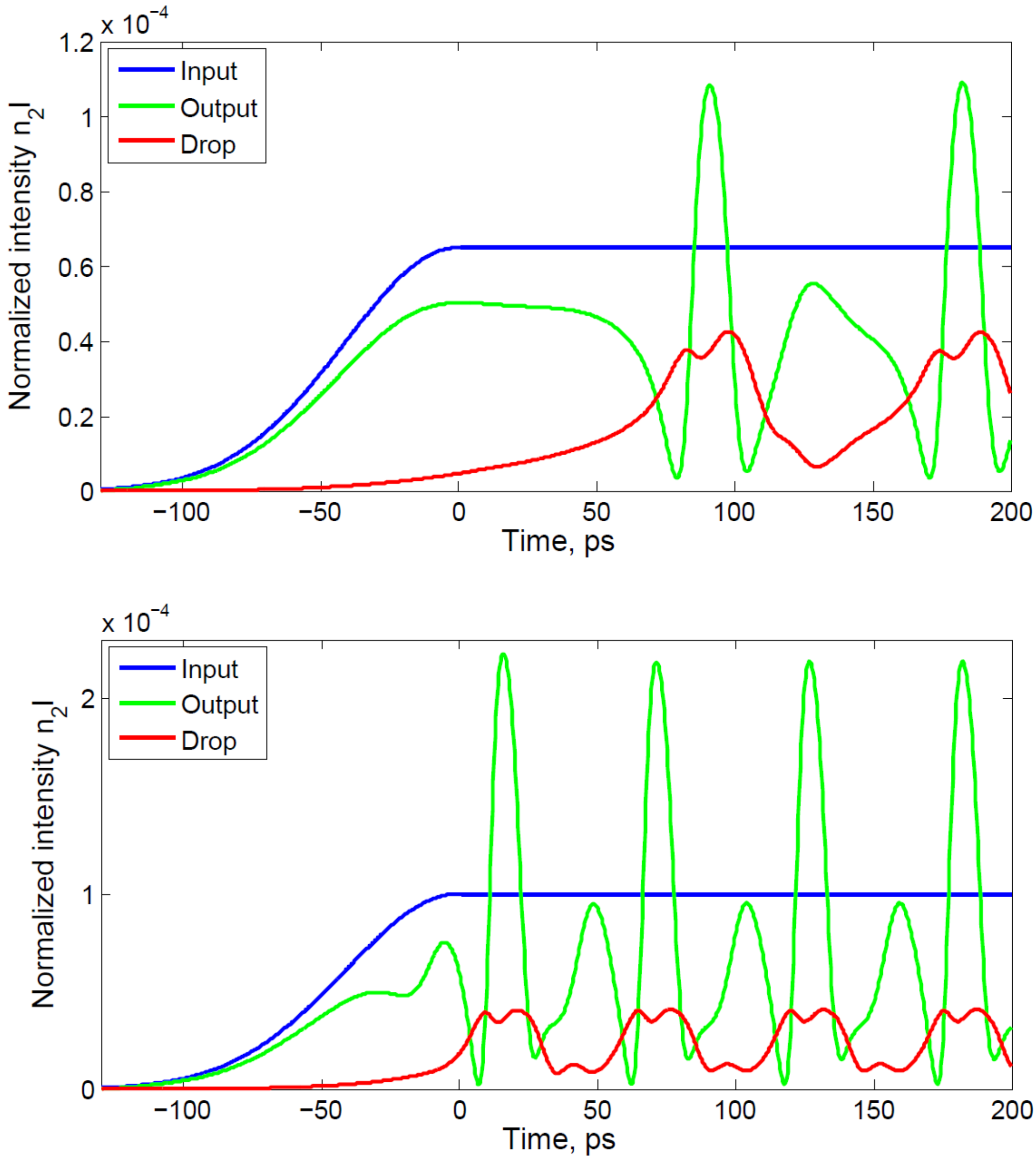

Figure 8: Time dependence of normalized intensity at input, through and drop ports for two levels of normalized input intensity in steady state $n_2 I_{in} = 6.5 \times 10^{-5}$, (a) and $n_2 I_{in} = 10^{-4}$ (b). The structure parameters are as in Fig. 7, detuning from resonance wavelength is $0.5\,n$m, [15]

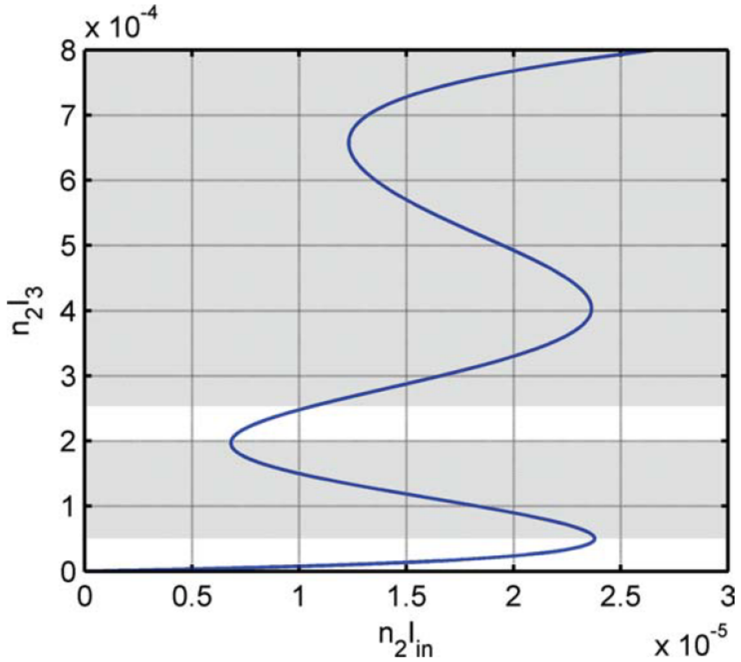

Figure 9: Normalized intensity in the third ring n_2I_3 as a function of normalized input intensity n_2I_{in}. Shaded regions represent intervals of n_2I_3 in which the solutions are unstable. The calculation parameters are described in the text, [16]

To understand the origin of these solutions, consider first Fig. 9. It is seen that most of the steady-state solutions are unstable. If the input intensity is kept constant, some of these solutions (usually in bistable or multistable regions, i.e., here for n_2I_{in} approximately between 6.8×10^{-6} and 10.5×10^{-6}) evolve until stable solutions are reached; the other unstable solutions (namely, for n_2I_{in} above 23.8×10^{-6}) evolve toward periodic (self-pulsing) or chaotic states. Note, that both kinds of solutions are possible if n_2I_{in} is located approximately between 10.5×10^{-6} and 23.8×10^{-6}. In this case, stable solutions can be numerically found simply by increasing the input intensity from level below 6.8×10^{-6}, whereas self-pulsing or chaotic solutions are obtained if the input intensity is decreased from initial value above $n_2I_{in} = 23.8 \times 10^{-6}$.

Thus, CE method, being a simple finite-difference scheme, can be used both for simulation of pulse propagation dynamics and for calculation of spectral dependencies. Namely, results, which demonstrate bistability, self-pulsing and chaos were presented.

3 Discrete-equation (DE) technique

In the previous examples we saw that for stable steady-state solutions the techniques CE and TMM provide exactly the same results (Fig. 7). It is known, that TMM treats the coupling as an immediate, a lumped one. In a nonlinear case this assumption becomes an approximation. However, previous examples show, that this approximation is well satisfied. Hence, there occurred a motivation to formulate another method, which is simpler than CE method and which assumes coupling as concentrated in one point - the discrete equation (DE) method. Despite different treating of the coupling region, the idea of separation the whole geometry of photonic structure on waveguides and waveguide couplers is common both for the CE and the DE methods.

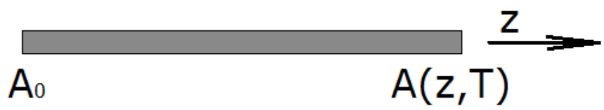

Figure 10: Single waveguide

3.1 Formulation for waveguide

Let us focus on an optical pulse propagation inside a single waveguide, Fig. 10. The initial intensity of pulse A_0 is known from the boundary conditions. In this section we formulate DE technique for finding the solution of Eq. (2.1) for calculation of intensity $A(z,T)$ at the arbitrary distanced point along the waveguide.

The Eq. (2.1) was derived for a case with instant response of nonlinear refractive index change. In the case when refractive index change is not immediate, it can be formulated as [6]:

$$T_R \frac{\partial \Delta n_{\mathrm{NL}}}{\partial t} + \Delta n_{\mathrm{NL}} = n_2 |A|^2, \tag{3.1}$$

where T_R is relaxation time and Δn_{NL} is nonlinear change of the refractive index. Consequently, the Eq. (2.1) for the delayed response gets more general form and is written as

$$\frac{\partial A}{\partial z} + \beta_1 \frac{\partial A}{\partial t} + \frac{\alpha}{2} A = i \Delta n A. \tag{3.2}$$

where $\Delta n = \Delta n_{\mathrm{NL}} \gamma / n_2$ is a nonlinear change of effective mode index. In this and further chapters we will use symbol n_2 (see Eq. 3.1) instead of symbol γ for denoting effective nonlinear coefficient (used in Eq. 2.1). The n_2 symbol was chosen, because it is used in great number of articles about these phenomena, [17], [18]. In Eq. 3.1 the Debye relaxation equation [19] was assumed.

The solution of Eqs. (3.2) and (3.1) is [2]:

$$A(z,t) = \exp\left(-\frac{\alpha}{2} z\right) A_0(t - \beta_1 z) \exp\left(i \eta (t - \beta_1 z) z_{\mathrm{eff}}\right); \tag{3.3}$$

$$T_R \frac{\partial \eta}{\partial t} + \eta = n_2 |A_0(t)|^2. \tag{3.4}$$

The solution provides explicit relation between amplitudes A_0 and A at different places of waveguide (see Fig. 10).

3.2 Formulation for ADF/APF structure

In previous section the single waveguide was discussed. Let us now consider more complicated structure consisting of N coupled ring resonators side coupled with two waveguides as shown in Fig. 11, (a). All the resonators are identical and made from the same single mode waveguide as the two waveguides. A_j, B_j, C_j and D_j represent the time-dependent (slowly varying) mode amplitudes at different positions in the rings or waveguides. The presented model is valid for unidirectional propagation of modes, i.e. the structure is excited at the input ('In') and/or add port. In the subsequent numerical calculations (Sections 3.4), however, we will always suppose excitation only at the input port, thus $C_{N+1} = 0$.

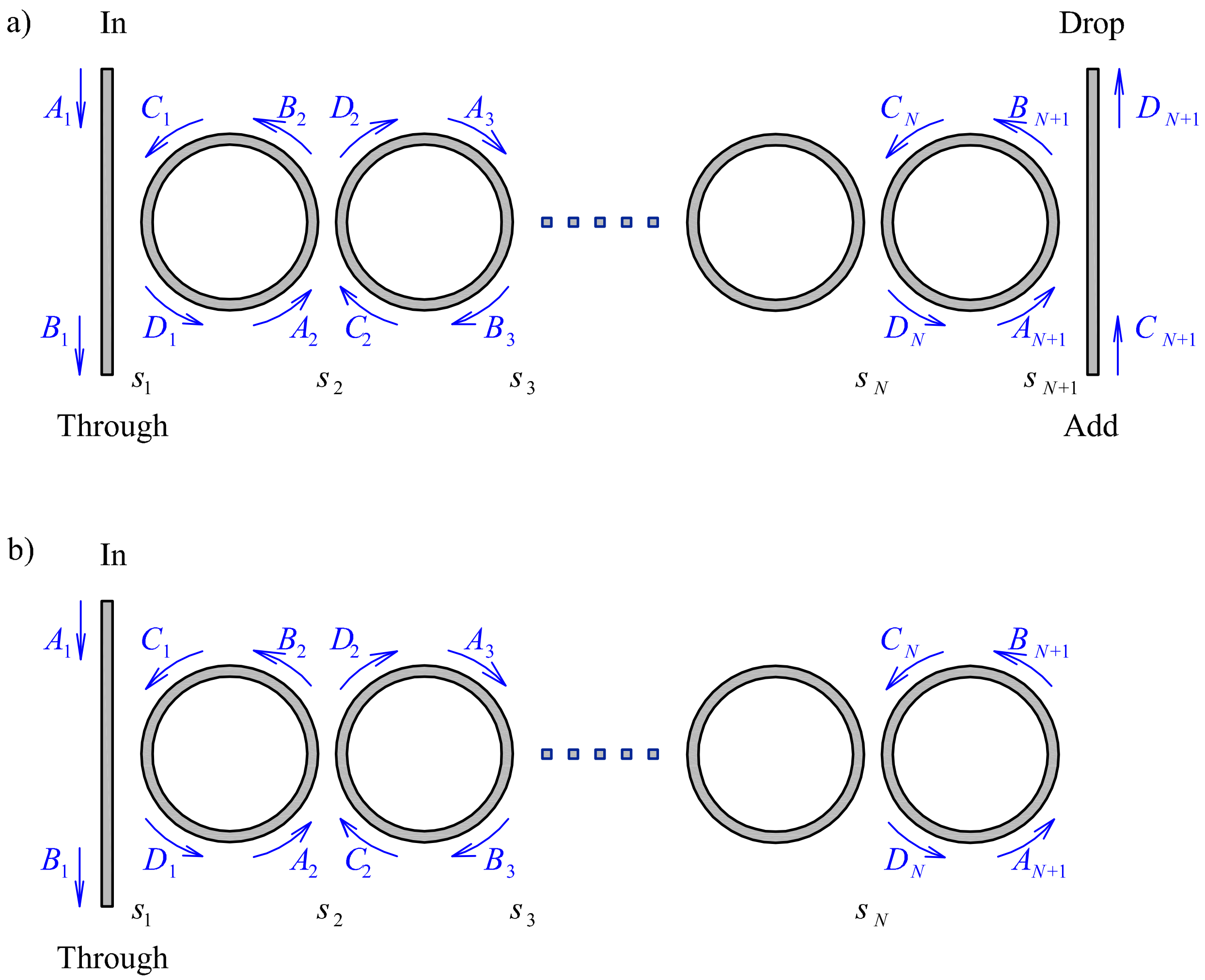

Figure 11: ADF (a) and APF (b) structures consisting of N coupled ring resonators. Each coupler is described by the parameter s_j.A_j, B_j, C_j and D_j represent mode amplitudes. Arrows indicate propagation of the modes

Similarly as in [20], [21] we assume that the coupling is lossless and localized at a single point. Then, by using the notation in Fig. 11, the interaction in each coupler (in time t) is given by

$$B_j(t) = r_j A_j(t) + i s_j C_j(t) \tag{3.5}$$

$$D_j(t) = i s_j A(t) + r_j C_j(t) \tag{3.6}$$

where is_j and $r_j = \sqrt{1 - s_j^2}, (j = 1, 2, \ldots, N+1)$ are respectively the coupling and transmission coefficients which describe each coupler, [20], [21].

The boundary conditions for optical pulse propagation are the following: if the ADF structure is studied, intensities A_1 and C_{N+1} at 'In' and 'Drop' ports respectively are known. In the case of APF only the input intensity A_1 is known. For the last ring in this structure, there is one more condition. In addition to the described above equations, amplitudes in the last resonator fulfill the relation:

$$B_{N+1}(t) = A_{N+1}(t). \tag{3.7}$$

The structure exhibits Kerr nonlinearity, i.e., in the stationary state, the nonlinear change of effective mode index at certain position in ring (or waveguide) is given by the relation of type $n_2 |A_j|^2$, where A_j is the physical amplitude of the mode at this position. However, instead of A_j we use dimensionless amplitude a_j defined by

$$a_j = \sqrt{\frac{2\pi}{\lambda_0} n_2 L_{\text{eff}}} A_j, \tag{3.8}$$

where L_{eff} is the effective length:

$$L_{\text{eff}} = [1 - \exp(-\alpha L)]/\alpha, \tag{3.9}$$

where L is the half of the ring circumference, α is the waveguide loss coefficient. The same scaling applies for the amplitudes b_j, c_j and d_j. In accordance with these definitions, we define powers at the input, through, and drop ports by the relations $P_{in} = (L/L_{\text{eff}})|a_j|^2$, $P_t = (L/L_{\text{eff}})|b_j|^2$ and $P_d = (L/L_{\text{eff}})|d_{N+1}|^2$, respectively. In this way, the powers are directly related to the physical amplitudes and can also be used as a measure of nonlinearity strength.

From Eq. (3.3) the the relations between mode amplitudes (Fig. 11) in the presence of Kerr-nonlinearity and waveguide loss can be derived:

$$c_j(t) = b_{j+1}(t - \tau_g) \exp\left[-\frac{\alpha L}{2} + i\phi + i\tilde{\beta}_{j+1}(t - \tau_g)\right], \tag{3.10}$$

$$a_{j+1}(t) = d_j(t - \tau_g) \exp\left[-\frac{\alpha L}{2} + i\phi + i\tilde{\delta}_j(t - \tau_g)\right]. \tag{3.11}$$

In these equations, $1 \le j \le N$, $\tau_g = n_g L/c$ is the the group delay corresponding to propagation of the pulse over distance $L.\phi = 2\pi n_{\text{eff}} L/\lambda_0$ is the linear phase shift acquired over distance L. The shift can be expressed as $\phi = \pi(m + \Delta f)/\text{FSR}$, where m is an arbitrary positive integer and Δf is the detuning from resonance. In the following analysis, we will always assume even m (adaption of the formulation for odd m is obvious) and thus ϕ in Eqs. (3.10) and (3.11) can be replaced by $\pi\Delta f/\text{FSR}$.

Nonlinear phase shifts $\tilde{\beta}_j$ and $\tilde{\delta}_j$ are given by the response of the medium. From Eq. (3.4) with the use of scaled amplitudes the following equations are derived:

$$T_R \frac{d\tilde{\beta}_j(t)}{dt} + \tilde{\beta}_j = |b_j(t)|^2, \tag{3.12}$$

$$T_R \frac{d\tilde{\delta}_j(t)}{dt} + \tilde{\delta}_j = |d_j(t)|^2. \tag{3.13}$$

The above system of the difference-differential equations Eqs. (3.5)-(3.13), which is a generalization of the Ikeda equations for a single ring [17], [18], fully describes the time evolution of the amplitudes a_j, b_j, c_j, d_j and nonlinear phase shifts $\tilde{\beta}_j$, $\tilde{\delta}_j$ from given initial conditions.

The system can be readily solved in the approximation of instantaneous response. In this case, we consider the limit $T_R \ll \tau$ and assume the solutions of Eqs. (3.12) and (3.13) in the form $\tilde{\beta}_j(t) = |b_j(t)|^2$ and $\tilde{\delta}_j(t) = |d_j(t)|^2$. Consequently, the whole system is reduced to a difference equations which appear, e.g. in [22].

For obtaining of the steady-state or time independent solutions of Eqs. (3.5)-(3.13), we assume no signal at the add port, $c_{N+1} = 0$ and arbitrarily choose the amplitude at the drop port d_{N+1}. Then, the other amplitudes are calculated step by step with using Eqs. (3.5)-(3.11), finally the amplitudes a_1 at the input and b_1 at the through port are found. Note that in the steady state, solutions of Eqs. (3.12) and (3.13) are formally the same as in the approximation of instantaneous response.

Otherwise, when it is needed to calculate the time evolution, the input amplitude a_1 is given and remained amplitudes are gradually calculated. Time evolution of unstable solutions can be obtained directly from equations (3.5) - (3.13).

3.3 Non-instantaneous response of the system

In the previous section the instantaneous response of the medium was discussed, i.e. the ratio of the relaxation time to the half ring round trip was neglected $T_R/\tau \ll 0$. Numerical experiments show, however, that this approximation may cause significant changes in the nature of solution [17], [19]. That is why in the general case of non-instantaneous response, we need an efficient technique for the numerical integration of Eqs. (3.12) and (3.13). This will allow us to make more precise map of structure states. Let us rewrite Eq. (3.12) here:

$$T_R \frac{d\tilde{\beta}_j(t)}{dt} + \tilde{\beta}_j = |b_j(t)|^2, \qquad (3.14)$$

compare with Eq. (3.4). Let us assume the solution of Eq. (3.14) in the form:

$$\tilde{\beta}_j(t) = |b_j(t)|^2 + \exp\left(-\frac{t}{T_R}\right) u(t). \qquad (3.15)$$

For numerical calculation, we approximate the integral of the exact solution of Eq. (3.14) by using the midpoint rule and apply discretization of the variable t with the step Δt. Hence, the approximate solution of Eq. (3.14) is obtained:

$$\tilde{\beta}_j(t+\Delta t) \approx |b_j(t+\Delta t)|^2 + \exp\left(-\frac{\Delta t}{T_R}\right)\left[\tilde{\beta}_j(t) - |b_j(t)|^2\right] - \\ - \exp\left(-\frac{\Delta t}{2T_R}\right)\left[|b_j(t+\Delta t)|^2 - |b_j(t)|^2\right]. \qquad (3.16)$$

The solution of Eq. (3.13) is calculated analogically. After substitution of these solutions to the Eqs. (3.10) and (3.11) a new equation system is obtained, calculation of which is straightforward.

Despite the ability of CE technique to provide time evolving of processes in optical structures, it can not directly define, whether the solution is stable or not. An analytic character of DE method readily makes it possible to apply the linear stability analysis and differentiate between stable and unstable solutions. To this aim we assumed the approximation of instantaneous response and calculated the eigenvalues of the Jacobian. The given solution is stable if and only if absolute value of any eigenvalue is less then 1, [18].

3.4 Numerical examples

Let us investigate the dynamical behavior of the ADF structure. The DE described technique can simulate a device with an arbitrary number of rings. However, with increasing number of rings, the structures exhibit more complicated behavior. Therefore, with the aim of obtaining tractable results and keeping minimal number of structural parameters, we present simulation of a simple structure with two rings.

Figure 12 shows steady-state solutions and their classification for the selected device. The systems optimized for flat-top response are not suitable for observing bistability, SP, and chaos, [13],

[23]. Therefore, we select the parameters s_j in such a way, that the device exhibits two resonance peaks ($P_d \approx P_{in}$), which are clearly seen in Fig. 12, (a). The behavior is similar to those observed in [23]. The peaks shift towards the negative values of the detuning as we increase nonlinearity strength (the power at the drop port P_d). The slope of the resonance regions is (approximately) equal to -1, which can be qualitatively explained by the linear increase of the effective mode index n_{eff} with P_d.

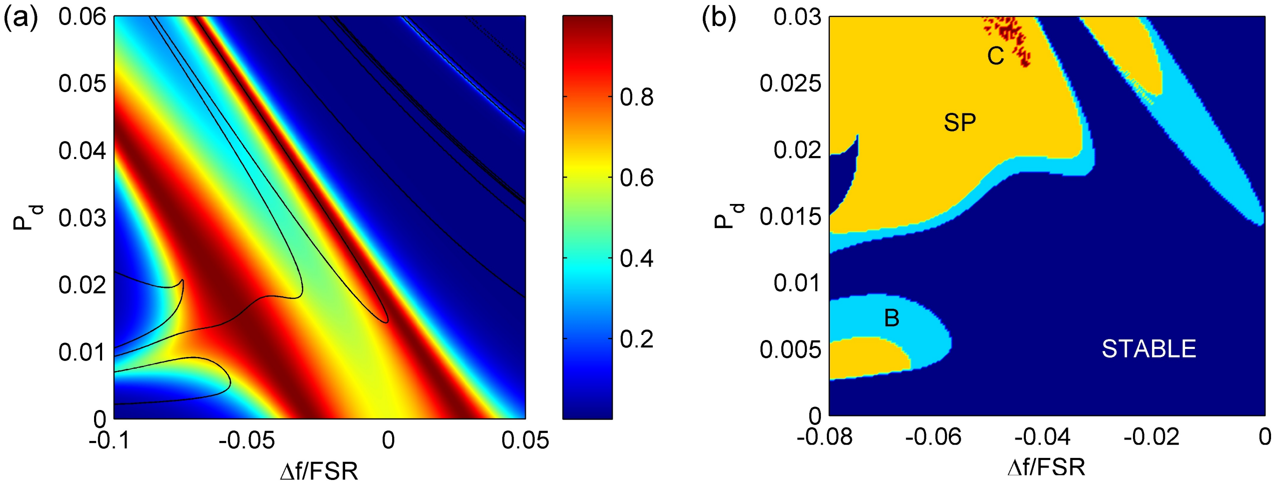

Figure 12: (a) Steady-state solutions for the ADF configuration. The color map indicates the relative power in the drop port. Solid lines denote boundaries between stable and unstable states. (b) Classification of the system, [24]

We evolve unstable solutions in time until we reach either stable, SP or chaotic solutions while keeping the input power P_{in} constant. The stable solutions belong to bistable (or multistable) region. In order to distinguish between SP (periodic) and chaotic solutions, we calculated autocorrelation of the signal at the drop port $D_3(t)$. In this way, we were also able to determine a period of the self-pulsations. Here, and in all the following examples, the calculation of the time evolution with non-instantaneous response was performed with the step $\Delta t = \tau/10$ and we also verified that this value has negligible influence on the presented results.

The control parameters are determined by input power P_{in}, dimensionless detuning Δ and coupling coefficients s_j. The steady state solutions of the ADF are shown for the various values of the power in the drop port P_d by relative power in the drop port P_d/P_{in}. The stable and unstable regions for the values $s_1 = s_3 = 0.42$, $s_2 = 0.2$ are presented in the Fig. 12.

The most interesting region for SP is found for negative detuning, bellow $\Delta f/\text{FSR} \approx -0.035$, and nonlinearity levels above $P_d \approx 0.02$. (SP states around $P_d \approx 0.005$ are not attractive because $P_d = P_{in}$ is small.) Note that the region extends next to the place where the resonance leaks into the gap. For the detuning bellow $\Delta f/\text{FSR} \approx -0.057$, the structure exhibits bistability (for nonlinearity levels $P_d \approx 0.007$) before reaching SP. Contrary to this, above $\Delta f/\text{FSR} \approx -0.057$, SP can occur without undergoing a bistable state. Chaotic states are found inside the SP region, near $P_d \approx 0.03$ and $\Delta f/\text{FSR} \approx -0.047$. The map of the ADF to show the stable, BS, SP, and chaotic regions with respect to P_d and Δ is shown in the Fig. 12, (b).

In order to examine the described behavior more closely, we consider $\Delta f/\text{FSR}$, which belongs to the mentioned bistable region, and present a bifurcation diagram in Fig. 13. [In our calculation, we, step by step, slightly increased (or decreased) P_{in}, fixed this value and searched for the corresponding stable, SP or chaotic state. As a initial condition, we used the state found for the previous value of

P_{in}. It should be noted that other solutions can be found for different ways of changing P_{in}.] As expected, we observe a bistable region followed by a Hopf bifurcation at $P_{in} \approx 0.016$, which is the birth of a limit cycle from the equilibrium, [25], [26] and suggests periodic oscillations. SP states are observed above the Hopf bifurcation and bifurcates into chaotic states at $P_{in} = 0.067$. Interestingly, there is a narrow region about $P_{in} = 0.066$ in which we observe either SP or chaos for increasing or decreasing of P_{in}, respectively. Note also that the unstable steady-states (gray shaded regions), which were identified by linear stability analysis with the approximation of instantaneous response, precisely correspond to the results of the exact calculation (green curve/area).

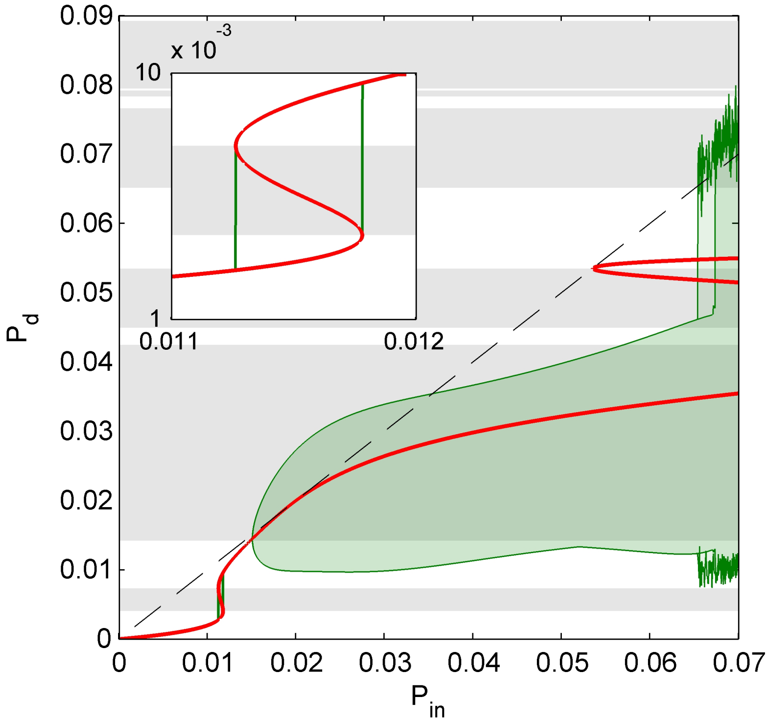

Figure 13: Power at the drop port P_d vs. input power P_{in} for $\Delta f/\text{FSR} = -0.06$; other structural parameters are as in Fig. 12. Green curve (area) labels values of P_d calculated for adiabatic increase and decrease of P_{in} (from 0 to 0.07 and back). Superimposed red curve shows steady-state solutions. Horizontal gray shaded regions mark intervals of P_d in which the steady-state solutions are unstable. Dashed line denotes 100% power transfer into the drop port, i.e., $P_d = P_{in}$. Bistable region is magnified in the inset

The behavior seen in Fig. 13 is characteristic for the given detuning. For example, as discussed before, the bistable region vanishes with increasing of $\Delta f/\text{FSR}$. On the other hand, decreasing of $\Delta f/\text{FSR}$ leads to a wider bistable region and finally to overlapping of SP and bistable regions.

An example of SP state is shown in Fig. 14 (a). Obviously, the period, amplitude (Fig. 13) and shape of pulses depend on the selected structure parameters. However, the pulses emerging from the through port have usually more complex shape than the pulses from the drop port. The corresponding phase portrait in Fig. 14, (b) demonstrates an attracting limit cycle; this calculation was obtained by evolving of the steady state found for the given P_{in} (at which $D_3 = 0.1604 + i0.0262$).

The effect of losses is demonstrated in Fig. 15. To this aim, we considered SP solutions and calculated the modulation depth, defined here as

$$\eta = [\max(P_d) - \min(P_d)]/(2P_{in}). \tag{3.17}$$

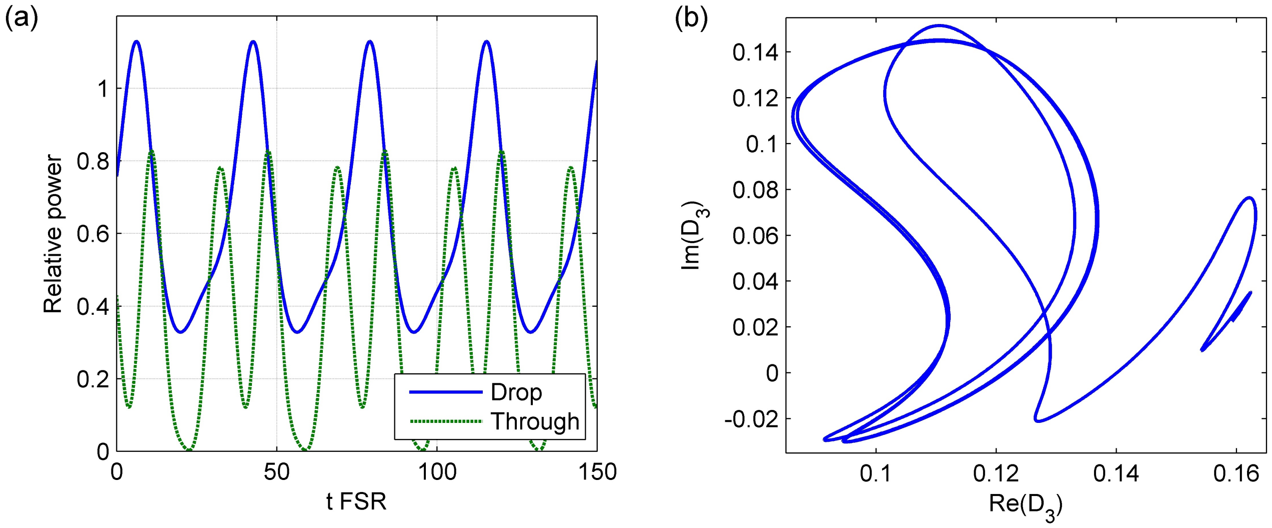

Figure 14: Time-domain solutions corresponding to SP region for $\Delta = -0.06$ with $s_1 = s_3 = 0.42, s_2 = 0.2, P_{in} = 0.03, \tau/T_R = 2$. (a) Relative powers in drop and through port vs normalized time. (b) Relative power in the rings

The loss is characterized with the parameter $\alpha' = \exp(-\alpha L)$. (Note that $\eta = 0$ corresponds to stable states. For chaotic states, observed for lossless case $\alpha' = 1, \eta$ is not shown in Fig. 15). It is seen, that the loss significantly affects the SP behavior, namely, it decreases the modulation depth and increases the threshold input power for SP. For $\alpha' \leq 0.93$ (approximately), we do not observe any SP for a given interval of input powers.

In Fig. 16 we demonstrate the influence of the input power of the SP period. This example also demonstrates the effect of finite relaxation time T_R on the SP behavior. For small values of τ/T_R, we observe period doubling followed by chaos. SP region increases with τ/T_R, namely due to the shift of the upper limit of P_{in}. (Chaotic states, that occur above this limit, are not shown in Fig. 16). With further increasing of τ/T_R, the period doubling vanishes, see the curve for $\tau/T_R = 2$, and the dependence approaches the results obtained in the approximation of instantaneous response, $\tau/T_R \to \infty$. However, this should be taken with caution; the approximation of instantaneous response can break down for longer time scales, [17]. As a result, more complicated SP behavior with period T FSR ≈ 1, (not shown in Fig. 16) is revealed when τ/T_R is increased above value about 3.

Finally, we compare our results with the phenomenological model that considers beating of the linear modes in coupled cavities, [27]. It follows from [27] that the period of SP can be estimated by using the formula $T = 2/(f_1 - f_2)$, where f_1 and f_2 are frequencies of the linear modes in two-cavity system. For our system, these frequencies correspond to the two peaks seen in Fig. 12 in the limit $P_d \to 0$. The calculated period, which is shown in Fig. 16 (horizontal dashed line), qualitatively well explain our exact results for the regime in which the approximation of instantaneous response can be applied.

To summarize, in this section the stability of two coupled rings structure was investigated by linear stability analysis. Steady-state solutions and their classification was presented. We identified suitable parameters for self-pulsing operation and demonstrated the self-pulsing state and the corresponding limit cycle. It has been demonstrated that unstable solutions can evolve towards SP states and for higher values of input powers we can observe chaotic states as well. The threshold input power for observing SP is strongly related by the amount of loss and/or the finite relaxation

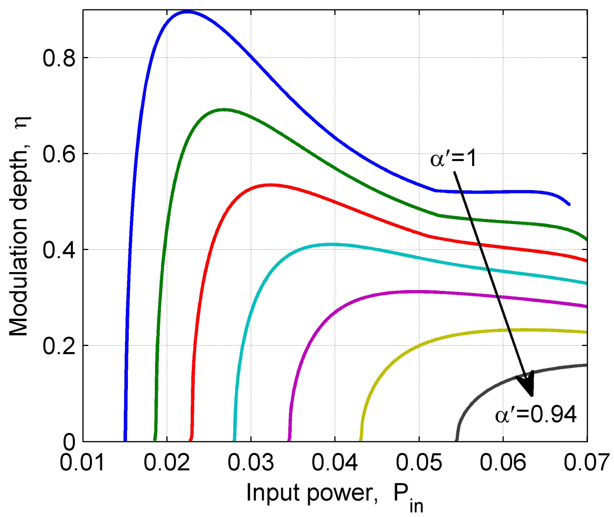

Figure 15: The modulation depth η vs. input power P_{in} for seven different values of the loss coefficient α' (1, 0.99, 0.98, 0.97, 0.96, 0.95 and 0.94); other structural parameters are as in Fig. 13. The arrow indicates the trend of increasing loss (decreasing α'). The dependencies were calculated for the adiabatic increase of P_{in}.

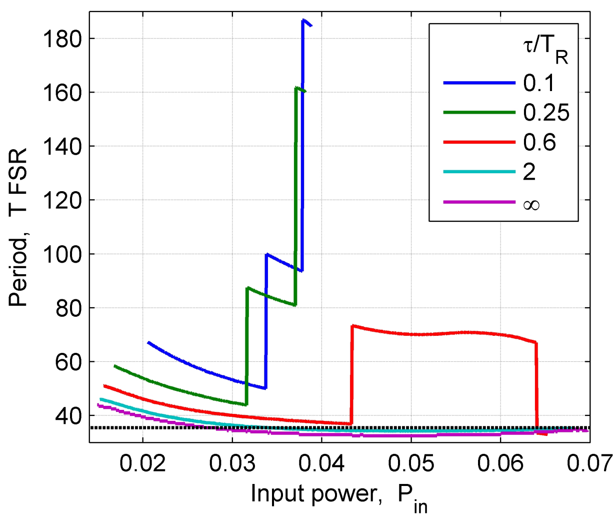

Figure 16: Normalized period T FSR of SP solution vs. input power P_{in} for the various values of τ/T_R shown in the legend; other structural parameters are as in Fig. 13. The black dashed line corresponds to the beating frequency of the two linear modes.

time in the CRRs. In addition, the self-pulsing period strongly changes with the finite relaxation time. In some circumstances, however, the period can be estimated by considering the beating of linear modes in coupled cavities, [27]. In presence of non-instantaneous Kerr response, the interval of the input power for having SP region becomes much shorter compare to the instantaneous Kerr response.

4 Conclusions

We developed two new approaches for simulation of pulse propagation in nonlinear waveguide structures.

The first technique - the Coupled Equations (CE) method - stems from the coupled mode theory. The technique uses a simple finite-difference scheme for solving of nonlinear coupled equations that describe propagation of optical pulses under slowly-varying envelope approximation, [8]. The developed scheme is based on the up-wind differencing, which provides stable and reliable solution of partial differential equations that describe pulse propagation [7].

The CE technique has been applied to Kerr-nonlinear structures with different geometries, [8], [15], [11], [16]. Microring resonators consisting of single or up to three rings coupled to one or two waveguides were simulated, [8], [11]- [16]. The analysis of the discretization of the equations on the base of our numerical experiments was made, [11]. The stability criterion and accuracy analysis were performed, [11], [16]. The comparison of the CE technique with the Transfer Matrix Method (TMM) method was made, [11], [15]. CE method showed good agreement with TMM. The phenomenon of self-pulsing in structures consisting of coupled ring resonators (CRR) was confirmed [14]. CE method main advantage is, that it enables easy inclusion of various nonlinear effects, thus suggesting that the technique may be considered as a useful counterpart of the established methods (such as mentioned above TMM or well-known Finite Difference-Time Domain method (FD-TD)).

The second developed technique - the Discrete Equations method (DE), is based on the difference equations that describe time-domain evolution of optical pulses inside the structure, [14]. Considering the coupling as instantaneous significantly reduces the time needed for simulation, comparing with CE technique, which increases the applicability of the method for accurate and fast simulations. The technique was generalized for the case of non-instantaneous system response, [24]. This allowed to enhance the precision of the solution map calculating. The performance of the method was presented on the example of Kerr-nonlinear coupled ring resonators both of APF and ADF configuration with two and three rings, [14], [24]. The stability of the system was investigated by considering linear stability analysis. The phenomenon of optical pulse generation from the continuous input was studied. It was demonstrated that unstable solutions can evolve towards self-pulsing (SP) states and for higher values of input powers, chaotic states can be observed as well, [24]. The dependence between input power for observing SP behavior and losses in the CRR was described, [24]. Also it was shown that in presence of non-instantaneous Kerr response, the interval of the input power for having SP region becomes much shorter compared to the instantaneous Kerr response, [24].

The presented results were published in two papers [16], [24] and in several conference contributions [8], [11], [14], [15].

One great challenge remaining in information technology today is to process optical signals directly in optical format. Nonlinear microring resonators play an important role in this concept. The results which were described in this work demonstrate ability of the developed numerical techniques to effectively deal with microring based structures. Thus, it is expected that further improvement and application of the techniques can contribute to highly innovative research of all-optical data processing devices.

References

[1] BOGAERTS W.; HEYN P.; VAERENBERGH T.; VOS K.; SELVARAJA S.K.; CLAERS T.; DUMON P.; BIENSTMAN P.; THOURHOUT D.; BAERTS R. Silicon microring resonators. *Laser Photonics Review*. 2011, 6, pp. 47-73.

[2] AGRAWAL G.P. *Nonlinear fiber optics*. 3rd edition. San Diego: Academic Press, 2001. pp. 466, ISBN 0-12-045143-3.

[3] YARIV A.; YEH P. *Photonics*. 6th edition. New York: Oxword Univercity Press, 2007. pp. 836, ISBN 0-19-517946-3.

[4] ALMEIDA V.R.; LIPSON M. Optical bistability on a silicon chip. *Optics Letters*. 2004, 29, pp. 2387- 2389.

[5] MARBURGER J.H.; FELBER F.S. Theory of a lossless nonlinear FabryPérot interferometer. *Physical Review A*. 1978, 17, pp. 335.

[6] AGRAWAL G.P. *Applications of Nonlinear Fiber Optics*. San Diego: Academic Press, 2001. pp. 458, ISBN 0-12-045144-1.

[7] PRESS W.H., et al. *Numerical recipies in Pascal. The art of science computing*. Cambridge: Cambridge Univercity Press, 1989. pp. 781, ISBN: 0-521-37516-9.

[8] STERKHOVA A.; PETRÁČEK J.; LUKSCH J. Simple numerical scheme for modelling of nonlinear pulse propagation in coupled microring resonators. In: *Proc. ICTON 2009*. ISBN: 978-1-4244-4826-5.

[9] BORISKIN A.V.; BORISKINA S.V.; ROLLAND A.; SAULEAU R.; NOSICH A. Test of the FEDE accuracy in the analysis of the scattering resonances associated with high-Q whispering-gallery modes of a circular cylinder. *Journal of the Optical Society of America A*. 2008, 25, pp. 1169- 1173.

[10] NIEGEMANN J.; PERNICE W.; BUSCH K. Simulation of optical resonators using DGTD and FDTD. *Journal of Optics A: Pure and Applied Optics*. 2009, 11, pp. 1- 10.

[11] STERKHOVA A.; LUKSCH J.; PETRÁČEK J. Analysis of coupled equation scheme for modelling of nonlinear pulse propagation in coupled microring resonators. In: *Proc. SPIE 7746*, 2010. ISBN: 987-0-8194-8236-5.

[12] LITTLE B.E.; CHU S.T.; HAUS H.A.; FORESI J.; LAINE J.P. Microring Resonator Channel Dropping Filters. *Journal of Lightwave Technology*. 1997, 15, No. 6.

[13] CHEN Y.; BLAIR S. Nonlinearity enchancement in finite coupled-resonator slow-light waveguides. *Optics Express*. 2004, 12, pp. 3353-3366.

[14] STERKHOVA A.; LUKSCH J.; PETRÁČEK J. Simulation of self-pulsing and chaos in coupled microring resonators. In *Proc. ICTON 2010*, ISBN 978-1-4244-7797-5.

[15] PETRÁČEK J.; STERKHOVA A.; LUKSCH J. Modelling of nonlinear pulse propagation in coupled microring resonators. In: *Proc. ICTON-MW 2009*, ISBN 978-1-4244-5745-8.

[16] PETRÁČEK J.; STERKHOVA A.; LUKSCH J. Numerical scheme for simulation of self-pulsing and chaos in coupled microring resonators. *Microwave and Optical Technology Letters*. 2011, 53, pp. 2238- 2242.

[17] IKEDA K.; DAIDO H.; AKIMOTO O. Optical turbulence: Chaotic Behaviour of Transmitted Light from a Ring Cavity. *Physical Review Letters*. 1980, 45, pp. 709-712.

[18] GIBBS H.M.; HOPF F.A.; KAPLAN D.L.; SHOEMAKER R.L. Observation of chaos in optical bistability. *Physical Review Letters*. 1981, 46, pp. 474-477.

[19] NEWELL A.C.; MOLONEY J.V. *Nonlinear Optics*. Canada: Addison-Wesley, 1992. pp. 436, ISBN 978-0-20-151014-0.

[20] POON J.K.S.; SCHEUER J.; MOOKHERJEA S.; PALOCZI T.P.; HUANG Y.; YARIV A. Matrix analisys of microring coupled-resonator optical waveguides. *Optics Express*. 2004, 12, pp. 90-103.

[21] YARIV A. Universal relations for coupling of optical power between microresonators and dielectric waveguides. *Electronics Letters*. 2000, 36(4), pp. 321-322.

[22] CHAMORRO-POSADA P.; MARTIN-RAMOS P.; SÁNCHEZ-CURTO J.; GARCÍA-ESCARTÍN J.C.; CALZADA J.A.; PALENCIA C.; DURÁN A. Nonlinear Bloch modes, optical switching and Bragg solitons in tightly coupled micro-ring resonator chains. *Journal of Optics A*. 2012, 14, 015205.

[23] MAES B.; FIERS M.; BIENTSMAN P. Self-pulsing and chaos in short chains of coupled nonlinear microcavities. *Physical Review A*. 2009, 80, pp. 033805-1 - 033805-7.

[24] PETRÁČEK J.; EKŞIOĞLU Y.; STERKHOVA A. Simulation of self-pulsing in Kerr-nonlinear coupled ring resonators. *Optics Communications*. submitted for publication.

[25] STROGATZ S.H. *Nonlinear Dynamics and Chaos with Applications to Physics, Biology, Chemistry and Engineering*. Cambridge, MA: Perseus Books Publishing, LLC, 1994. pp. 512, ISBN 0-7382-0453-6.

[26] HALE J.; KOÇAK. *Dynamics and Bifurcations*. New York: Springer-Verlag, 1991. pp. 592, ISBN 978-0-38-797141-4.

[27] GRIGORIEV V.; BIANCALANA F. Resonant self-pulsations in coupled nonlinear microcavities. *Physical Review A*. 2011, 83, p. 043816.

Curriculum Vitae

Name: Anna Sterkhova
Date of birth: 18.03.1985
Contact: anna.sterkhova@seznam.cz

Education

2007 – today	**Brno University of Technology, Faculty of Mechanical Engineering. Department of Physical Engineering** Ph.D. study on modelling of pulse propagating in nonlinear photonic structures. State exam passed in May 2011.
2006 – 2007	**Brno University of Technology, Faculty of Mechanical Engineering. Department of Manufacturing Technology** State exam passed in June 2007. Master thesis: Progressive methods for machining of titan alloys

Job experience

08/2012 – today	Title:	Process engineer
	Company:	IMI International – Norgren CZ, s.r.o.
11/2010 –	Title:	Process engineer
07/2012	Company:	Tyco Electronics EC Trutnov s.r.o.
2005 – 2006	Title:	Technologist
	Company:	„Izhevskiy Radiozavod“ (Izhevsk, Russia)

Languages:

Russian, Czech, English

Abstract

The demand for more effective data-storage and faster signal processing is growing with every day. That is why the attention of the scientists is focused on the all-optical devices, which can improve the above mentioned requirements. Microring optical resonators are among the state of art devices, that are under consideration. There is a variety of numerical techniques to simulate processes occurring while the optical signal propagates in the microring resonator structure. They differ in its calculation effectivity, used approximations and possibilities of application. The aim of this work was to develop two simple and practical numerical methods for simulation of pulse propagation in nonlinear waveguide structures. It was also demanded, that opposed to the commonly known and frequently used finite-difference time-domain (FD-TD) method, the newly developed techniques could be easily applicable for the study of nonlinear structures based on microring resonators. That is why developed methods use some approximations, namely the slowly varying envelope approximation. The methods advantage is high speed and low requirements of computational resources.

Both techniques are based on observation that waveguide structures that use microring optical resonators can be considered as a single waveguide and the waveguide coupler. The first numerical technique solves coupled partial differential equations, which describe pulse envelope propagation in the structure. In order to obtain numerically stable formulation, this method uses the "up-wind" scheme, which is suitable for the partial differential equations that describe the wave propagation.

The second developed technique is derived from the first one. The difference between methods is in the treatment of the coupling between two waveguides. If in the first method the coupling is considered as the real one, distributed on the given length, in the second method the coupling is considered to be concentrated in one point. Due to this approximation it is possible to integrate the corresponding equations and achieve significant increase of calculation speed. Quasianalytical character of the second method enables also easy identification of different types of steady-state solutions. Due to these properties the second method was used to study spontaneous generation of optical pulses in the structures, consisting of coupled ring resonators.

Both methods, which were developed during this work, represent fast and physically illustrative alternatives to the FD-TD, so it can be expected that these methods can play an important role during the research of nonlinear waveguide structures.

Abstrakt

V současnosti jsme svědky stále zvyšujících se nároků na rychlost přenosu a zpracování signálu a kapacitu pamět'ových zařízení. Proto se pozornost výzkumných pracovníků zaměřuje k plně optickým zařízením, která by mohla splnit zmíněné požadavky. Jednou z intenzívně zkoumaných možností je využití mikroprstencových optických rezonátorů. Při výzkumu je nutné využít numerických metod, které simulují šíření optického záření v dané struktuře. K tomuto účelu existuje celá řada metod, které se liší v efektivitě výpočtu, použitých aproximacích, i možnostech použití. Cílem této práce bylo vyvinout dvě jednoduché a praktické numerické metody pro modelování šíření pulzního záření v nelineárních vlnovodných strukturách. Přitom bylo požadováno, aby, na rozdíl od obecně známé a často využívané metody konečných diferencí v časové oblasti (FD-TD), bylo možné metody snadno aplikovat při studiu nelineárních struktur založených na mikroprstencových rezonátorech. Proto vyvinuté metody používají některé aproximace, zejména aproximaci pomalu

proměnné obálky. Výhodou metod je vysoká rychlost a skromné požadavky na výpočetní zdroje.

Obě metody vycházejí ze skutečnosti, že naprostá většina nelineárních struktur založených na mikroprstencových rezonátorech se skládá ze dvou základních prvků: obyčejných vlnovodů a vlnovodných vazebních členů. První metoda řeší vázané parciální diferenciální rovnice, které popisují šíření obálky pulzu ve struktuře. Přitom je použito tzv. "up-wind" schéma vhodné pro parciální diferenciální rovnice popisující šíření vln.

Druhá metoda vychází z první; rozdíl je v popisu vazby mezi dvěma vlnovody. Pokud se v první metodě uvažuje realistická vazba rozložená na určité délce, pak druhá metoda je založena na představě vazby nacházející se v jednom místě. Díky tomu je možné integrovat příslušné rovnice a dosáhnout výrazného urychlení výpočtu. Kvazianalytický charakter druhé metody umožňuje dále snadnou klasifikaci různých typů ustálených řešení. Vzhledem k těmto vlastnostem byla druhá metoda využita k výzkumu samovolné generace optických pulzů ve strukturách skládajících se z vázaných prstencových rezonátorů.

Obě metody, které byly vyvinuty během této práce, představují rychlé a fyzikálně názorné alternativy k metodě FD-TD, a tak lze očekávat, že mohou hrát důležitou roli při výzkumu nelineárních vlnovodných struktur.